Effect of He implantation on the microstructure of zircaloy-4 studied using *in situ* TEM

M.A. Tunes[a,*], R.W. Harrison[a], G. Greaves[a], J.A. Hinks[a], and S.E. Donnelly[a]

[a] *School of Computing and Engineering*
University of Huddersfield
HD1 3DH, Huddersfield
United Kingdom

Abstract

Zirconium alloys are of great importance to the nuclear industry as they have been widely used as cladding materials in light-water reactors since the 1960s. This work examines the behaviour of these alloys under He ion implantation for the purposes of developing understanding of the fundamental processes behind their response to irradiation. Characterization of zircaloy-4 samples using TEM with *in situ* 6 keV He irradiation up to a fluence of 2.7×10^{17}ions $\cdot$ cm^{-2} in the temperature range of 298 to 1148 K has been performed. Ordered arrays of He bubbles were observed at 473 and 1148 K at a fluence of 1.7×10^{17}ions $\cdot$ cm^{-2} in αZr, the hexagonal compact (HCP) and in βZr, the body centred cubic (BCC) phases, respectively. In addition, the dissolution behaviour of cubic Zr hydrides under He irradiation has been investigated.

Keywords: Radiation damage, Zirconium alloys, *In situ* ion irradiation, Hydrides, Bubble lattices

1. Introduction

Zirconium alloys have been widely used in the nuclear industry since the 1960s as nuclear fuel claddings because of their corrosion resistance, low thermal neutron absorption cross sections and their desirable mechanical properties [1–6].

In a nuclear reactor, neutron irradiation causes changes to the microstructure and properties of both structural and fuel materials. In the case of Zr alloys, it has been reported that dislocation loops are the most common type of damage observed which increase in size and decrease in density with increasing neutron irradiation temperature [7]. The formation and growth of vacancy-type dislocation loops [8] has been associated with the swelling of zircaloy-2 and -4 by Griffiths *et al.* [9]. Gilbert *et al.* observed in post-irradiated zircaloy-2 that (n,α) transmutation reactions, mainly from ^{10}B and O impurities, lead to the preferential nucleation of cavities on grain boundaries [7]. The low concentration of He, presence of dislocation loops, low energy

*Corresponding author: Tel. +44 01484 471689
Email address: M.A.Tunes@hud.ac.uk (M.A. Tunes)

for vacancy formation and relatively-high atomic volume of Zr have been connected with the absence of voids in neutron irradiated Zr and its alloys [4, 7, 10, 11].

Ion beam irradiation has been applied as a powerful technique to test alloys and other materials prior to their use in nuclear reactors [12]. As well as avoiding the hazards associated with induced radioactivity, it is possible to reach the damage levels of a conventional light-water reactor ($\approx$2 dpa[1]$\cdot$year^{-1} [13]) in minutes to hours compared to rates in materials test reactors of between 10 to 20 dpa$\cdot$year^{-1} [12]. By careful selection of the ion irradiation parameters such as damage rate and temperature, it is possible to simulate the conditions experienced in a nuclear reactor [12, 14].

One area of particular interest has been the implantation of inert gases such He, Xe and Ar into metals [15] and much work has been done for many different systems including iron and its alloys [16], tungsten [17–19], copper [20], nickel [21], molybdenum [22, 23] and carbon [24] which are important for both fission and fusion reactors.

There have been numerous studies looking into the effects of irradiation on Zr alloys [4–6, 25, 26]. Ran *et al.* [27] studied the effects of 800 keV Kr ions on the microstructure of the alloy Zr-Nb-Fe-Cu-Ni observed via transmission electron microscopy (TEM) during *in situ* annealing after irradiation at temperatures from 700 to 1225 K. The authors reported that the size of Kr bubbles was strongly dependent on the annealing temperature and time: bubbles were observed with diameters of around 2.1 nm at 700 K, 2.7 nm at 875 K and 8.9 nm at 1140 K after 180 minutes of annealing. An exponential empirical formula was proposed for the growth behaviour which was attributed to the increased mobility of Kr ions in the βZr phase.

Pagano *et al.* [28] performed 650 keV Kr irradiation *in situ* within a TEM on four different Zr alloys. Bubble formation was observed in all four alloys and at all irradiation temperatures. However, no clear relationship was found between the bubbles sizes and the irradiation temperature in the range from 573 to 973 K.

Some studies have addressed the effects of He implantation on the microstructure of Zr alloys. Zee *et al.* [29] reported the occurrence of blisters on the surface of Zr-2.5Nb (wt.%) alloy during 50 keV He implantation at temperatures from 100 to 773 K. They concluded that when the alloy is cold worked prior to irradiation, βNb precipitates could act as trapping sites resulting in the development of He bubbles at a fluence of 5×10^{17}ions $\cdot$ cm^{-2}. Another *in situ* TEM annealing study was performed by Shen *et al.* [30] with the alloy Zr-Sn-Nb-Fe-Cr. They irradiated with 400 keV He ions and observed that the mean size of the He bubbles increased with irradiation temperature from 300 to 1173 K and with He fluence from 0.5×10^{17} to 5×10^{17}ions $\cdot$ cm^{-2}.

In addition to studies of bubbles in Zr alloys, several papers have aimed to understand the behaviour of Zr hydrides (ZrH) which may lead to delayed fracture and embrittlement in Zr alloys under in-service conditions [31–35]. Hydrides are stable or metastable compounds of the

[1]Displacement-per-atom or dpa: at one dpa every atom has, on average, been displaced from its lattice site once.

ZrH system and are preferentially formed at grain boundaries during both cooling and corrosion processes [36]. Metallic hydrides are brittle, exhibiting high thermal conductivity, high electrical resistance, high hardness and are often associated with the embrittlement in Zr alloys [37]. Below 873 K, the stable phase of the ZrH system is δ which has a face-centred cubic (FCC) structure with a H content from 0 to 62 at.%. Two other phases are reported: the face-centred tetragonal (FCT, the γ-phase) which is a metastable phase observed below 873 K in the same H content range as the δ-phase, and the ϵ-phase which is also FCT and occurs when the H content is higher than 64 at.% at temperatures below 973 K [37, 38].

Carpenter and Waters [39] performed an *in situ* TEM annealing study to explore the dissolution of γ hydrides up to 700 K. After annealing, the incomplete dissolution of hydrides was concluded to increase the dislocation density. The authors also performed *in situ* TEM electron irradiation of Zr to a dose of 0.065 dpa at room temperature showing that the irradiation can prevent dislocations from annihilating during thermal dissolution. The observed effect of dislocation pinning was associated with the formation of point defect clusters and jogs induced by the electron irradiation.

To date, there have been no studies which have used the technique of TEM with *in situ* He ion implantation to explore the microstructural evolution of Zr alloys. In this work, a TEM study with *in situ* ion irradiation has been performed on zircaloy-4 under 6 keV He bombardment. The irradiated samples have been examined at four temperatures within the range from 298 to 1148 K so as to match the temperatures of a LWR under normal operation and during loss of coolant scenarios and to investigate the differences in the damage microstructure of the αZr, βZr and δZrH phases.

2. Materials and methods

2.1. Samples studied

The material used in this work was zircaloy-4 with the composition Zr-1.45Sn-0.2Fe-0.1Cr (wt.%) and a melting point (T_m) of 2123 K. Prior to the TEM sample preparation, the alloy was chemically etched with a solution containing 5% of HF, 35% of HNO_3 and 60% of deionised water (vol.%). Optical micrographs after etching revealed the presence of equiaxed grains which may indicate that the alloy was cold worked and then annealed.

2.2. TEM sample preparation

Samples 3 mm in diameter were punched from a thin foil and mechanical polishing was performed using SiC paper from 120 to 1200 grit in order to reduce the thickness. The samples were electropolished using a Struers TenuPol-5. A recipe from [40] was adapted for use with this system: an electrolyte of 10% of $HClO_4$ and 90% of CH_3OH (vol.%) at a bath temperature of 233 K with a flow rate set to 30 (arbitrary units as indicated on the TenuPol-5 display). Electropolishing was performed to perforation and the samples were then washed in methanol and dried in air. Figure 1 shows a high-resolution TEM image obtained after the sample preparation.

2.3. In-situ irradiation and annealing within a TEM: MIAMI-1 facility

Specimens were irradiated with 6 keV He ions *in situ* within a TEM at four temperatures: 298 ($0.14T_m$), 473 ($0.22T_m$), 973 ($0.45T_m$) and 1148 K ($0.54T_m$) using a double-tilt heating holder in a JEOL JEM-2000FX operating at 200 kV in the MIAMI-1 facility at the University of Huddersfield [41]. The ion flux was $9.6\times10^{13}\text{ions}\cdot\text{cm}^{-2}\cdot\text{s}^{-1}$ measured at the specimen position. The TEM samples were horizontal in the microscope with the ion beam at 30° from the electron beam. Images and videos were captured using a Gatan ORIUS SC200 digital camera. Through-focal imaging was performed in order to optimally image bubbles with defocus of ±96 nm and their sizes were measured using the software ImageJ [42].

The Monte-Carlo computer code *Stopping and Range of Ions in Matter* (SRIM) [43] was used to calculate the damage profile following the procedure suggested by Stoller *et al.* [44]. This yielded a damage level of 16 vacancies per incident ion which was used to convert fluences into dpa using 100 nm as the sample thickness. In this work, the zircaloy-4 samples were irradiated up to a fluence of $2.7\times10^{17}\text{ions}\cdot\text{cm}^{-2}$ corresponding to 5.0 dpa.

3. Experimental results

3.1. Zr hydrides

Hydrides were observed as precipitates in the matrix, preferentially located near to grain boundaries, and exhibited needle-like elongated shapes with lengths varying from 0.1 to 3 μm. Their presence in the samples is attributed to H pick-up during the electropolishing [36, 38, 40].

Figure 2 features TEM micrographs of a hydride with a length of around 500 nm. Note that the diffraction pattern has two different crystalline zone axes: one corresponding to the αZr phase and another to the δZrH phase. A dark-field image (figure 2b) obtained using the $(00\bar{2})$ reflection from the hydride (figure 2c) and confirms its crystalline nature.

Indexing was performed using the JCPDS database [45] and additional references available in the literature [46, 47]. Hydrides were indexed as being FCC corresponding to the δ-phase as reported previously [38]. The elongated geometry and diffraction patterns were in agreement with observations of similar precipitates in the literature [37].

3.1.1. In-situ annealing behaviour

An annealing experiment was performed in order to assess the hydride stability with increasing temperature. Figure 3a shows a zircaloy-4 microstructure featuring hydrides with size lengths varying from 0.01 to 2 μm at room temperature. Figures 3b to 3d show the same microstructure as the temperature increased from 273 to 673 K: all the hydrides were thermally dissolved at around 823 K. According to the ZrH phase diagram reported by Zuzek *et al.* [48], no hydride precipitation is expected in Zr above temperatures of around 823 K. Figure 3e shows the resulting microstructure clear of hydrides at 1148 K after annealing.

3.1.2. Hydride stability under in situ irradiation

As the hydrides were found to be thermally stable at temperatures below 650 K, two experiments were performed with 6 keV He ions at room temperature and at 473 K to assess their behaviour under irradiation. At room temperature and a fluence of 1.7×10^{17}ions $\cdot$ cm^{-2} (3.2 dpa), it is evident from figure 4 that the Zr hydrides remain stable under irradiation. However, preferential nucleation and growth of He bubbles at ZrH-Zr interfaces was observed.

In a different experiment, the irradiation-induced dissolution of Zr hydrides was observed at the irradiation temperature of 473 K. Figure 5a shows three hydrides at a grain boundary. As the fluence increased, the hydrides were observed to slowly dissolve in the αZr matrix and after 1.6×10^{17}ions $\cdot$ cm^{-2} (3.0 dpa), the phase transition was complete. Figure 5d shows the microstructure after irradiation with no hydrides observable however, residual "skeletons" could be seen at the original locations of the dissolved hydrides.

3.2. The effect of temperature on damage microstructure of zircaloy-4

In contrast to the observations following irradiation at 273 K, at 473 K one-dimensional bubble lattices (also referred to as bubble rafts) were observed after the hydride dissolution. In this case, a bubble lattice was observed in the αZr with the phase confirmed by the diffraction pattern shown in figure 6c. Figures 6a and b show bubble lattices at 1.7×10^{17}ions $\cdot$ cm^{-2} (3.2 dpa) and 2.6×10^{17}ions$\cdot$cm^{-2} (4.8 dpa), respectively. The upper insets in figures 6a and b are fast Fourier transforms (FFTs) of the images with the bright lobes corresponding to the orientation and periodicity of the bubble lattice.

In another experiment on the αZr matrix at 973 K, bubbles became observable in the TEM at a fluence of around 5.4×10^{16}ions$\cdot$cm^{-2} (1.0 dpa) and grew as the damage increased as shown in figure 7. However, at this temperature no bubble lattices were observed.

On increasing the temperature to 1148 K and thus above the $\alpha \longrightarrow \beta$ massive phase transition at 1120 K [49], a bubble lattice was also observed to form at a fluence of approximately 1.1×10^{17}ions $\cdot$ cm^{-2} (2.1 dpa). Figure 8 shows the evolution of the microstructure of zircaloy-4 during irradiation. Figure 8d is the diffraction pattern of the βZr phase indexed with parameters from the literature [45]. The FFT insets indicate that the bubble lattice orientation changed as the fluence increased due to tilting of the thin foil during the irradiation.

It was possible to assess the bubble growth behaviour as a function of the irradiation temperature by measuring the size of bubbles in the zircaloy-4 irradiated microstructures. Figure 9 shows that the sizes of the bubbles were approximately the same when bubble lattices were observed at 473 K (in the αZr phase) and 1148 K (in the βZr phase) at a fluence of 1.7×10^{17}ions $\cdot$ cm^{-2} (3.2 dpa).

Coalescence of bubbles was observed in the experiments at 973 and 1148 K when the fluence exceeded 1.6×10^{17}ions $\cdot$ cm^{-2} (3.0 dpa). Figures 7c and 8c show the zircaloy-4 microstructure at these temperatures at 2.7×10^{17}ions $\cdot$ cm^{-2} (5.0 dpa). When the fluence was increased from 1.6×10^{17}ions $\cdot$ cm^{-2} to 2.7×10^{17}ions $\cdot$ cm^{-2}, bubbles continued to grow and the average

sizes at 973 and 1148 K were approximately 5.5 nm and 8.9 nm, respectively. Although the bubble lattices were formed in both the αZr and βZr phases at 473 and 1148 K, respectively, the phenomenon was not observed at 298 and 973 K during implantation of the αZr phase. Figure 9 compares the average bubble sizes at the four different temperatures and at fluences of 1.7×10^{17}ions $\cdot$ cm^{-2} (3.2 dpa) and 2.7×10^{17}ions $\cdot$ cm^{-2} (5.0 dpa).

4. Discussion

Hydrides are formed when the H concentration exceeds the terminal solid solubility of Zr [38]. The presence of ZrH in the microstructure of Zr alloys leads structural components of LWRs to fail by several possible mechanisms as reported in the scientific literature. These include delayed hydride cracking [32–34], H-related fracture [50] and embrittlement [35].

Under in-service conditions, corrosion of Zr alloys can take place in a LWR [1, 51]. This causes the release of H which is able to diffuse throughout the matrix where it remains in solid solution resulting in a stable or metastable precipitate [33]. The current work shows that He implantation has a significant effect on the Zr hydrides: at 473 K they are slowly dissolved with He bubbles nucleating and growing after the dissolution (figures 4 and 5). This process was found to be different from the thermally-assisted dissolution during annealing as observed in the experiment shown in figure 3. Under the experimental conditions used in the current work, the thermally-assisted dissolution was faster and occurred at a higher temperature compared to the irradiation-assisted dissolution.

In contrast to the work of Carpenter *et al.* [39], the current work at 298 K showed that the He bubbles started to accumulate around ZrH-Zr interfaces prior to irradiation-induced dissolution. At this temperature, the diffusional mechanism of He trapped in vacancies is due purely to direct collisional displacements of lattice atoms promoted by the ion irradiation [52] as depicted in figure 10a(i). The dense dislocation networks surrounding hydrides as reported by Carpenter *et al.* [39] were not observed in the current work.

When the hydrides dissolved under ion irradiation in the experiment at 473 K, the He diffusivity in the matrix is believed to be characterised by a combination of direct displacements and replacements as studied by Trinkaus *et al.* [52]. The latter mechanism occurs when a substitutional He atom is converted into an interstitial atom due to its replacement by a self-interstitial atom as depicted in figure 10a(ii).

In the current work, the experimental evidence suggests that a combination of different mass-transport mechanisms play roles in the hydride irradiation-assisted dissolution at 473 K. As the fluence increased at 473 K, direct displacements, replacements and self-interstitial diffusion are all expected to have contributed to the knock-out of hydrogen atoms from the ZrH precipitate leading to the irradiation-assisted dissolution [52]. The dissolution was not observed at 298 K at which temperature only the displacement diffusion mechanism takes place with irradiation. Figure 10b is a schematic of the He diffusional mechanisms in solids proposed by Trinkaus *et al.* for the case of ZrH irradiation-induced dissolution.

The bubble lattice phenomenon was first reported by Sass and Eyre in 1973 [53, 54]. Various mechanisms have been proposed to account for bubble lattice formation including elastic interactions between the bubbles [55]. A bubble lattice in Zr was reported by Evans and Mazey [56] due to Kr implantation at 673 K in which they associated the two-dimensional anisotropic diffusion of self-interstitials atoms (SIA) with the ordering phenomenon and some more-recent computer simulations have attempted to shed light on the issue [57, 58].

The current work reports the observation of He bubble lattices in zircaloy-4 at 473 K and 1148 K in two different crystalline structures (HCP and BCC). The bubble ordering in zircaloy-4 was found not to be three dimensional, but rather the bubbles were aligned in planes or rafts in agreement with previous observations [56]. For both the αZr and βZr phases, the average bubble size was similar which therefore indicates that the physical dimensions of bubbles in an ordered array are not dependent on the structure of the parent Zr phase.

According to Thompson [59], the equilibrium condition for a gas bubble in a solid is when the rates of arrival and departure of vacancies and He at a given bubble are exactly the same and this will occur at a specific size of bubble. At this equilibrium, a gas bubble does not shrink or grow. This suggests that when bubble lattices were observed in both αZr and βZr at different temperatures, the equilibrium condition was the same in each case as the measured sizes of He bubbles are similar. This is not the case when bubble lattices were not observed at 298 K and 973 K.

A further interesting finding of the experiments presented here is the wide range of temperatures and two crystallographic phases in which bubble lattices were observed to form. Vacancies are expected to be immobile at 298 K and mobile at 1148 K [52, 60, 61]. Furthermore, both the mechanisms and the rates of He diffusion are known to be governed by the effects of temperature and irradiation [52]. Therefore, interstitials will be the point defect species which exhibit most consistency of behaviour being rapidly mobile at both temperatures at which bubble lattices were observed to form suggesting that they may be the critical driving force for the ordering mechanism. Whether or not the diffusion of self-interstitials may be critical to the formation of He bubble lattices in zircaloy-4, as suggested by Evans and Mazey for Kr bubble lattices in Zr at 673 K [56], is the subject of ongoing further investigations.

5. Conclusions

In this work, a study of He ion implantation of zircaloy-4 was performed *in situ* within a TEM. The differences between the αZr and βZr phases have been discussed in terms of irradiation fluence and temperature. The major outcomes of this work can be summarized as follows:

- The stability of Zr hydrides during irradiation was studied. The irradiation-induced dissolution of hydrides was observed at 473 K and to have completed by a fluence of 1.7×10^{17}ions $\cdot$ cm^{-2} (3.2 dpa). The mechanism is suspected to be different from that for thermal dissolution reported by previous authors.

- A combination of atomic displacement and replacement mechanisms allowed the diffusion of He in Zr under irradiation is suggested as a possible explanation for hydride dissolution observed at $0.22T_{\mathrm{m}}$.

- Bubble lattices were observed to form during irradiation at 473 and 1148 K in two different crystalline phases (αZr and βZr) at around the same fluence. In the latter case of 1148 K, the diffusion of vacancies and interstitials is faster than at 473 K and the observation of bubble lattices has not been reported previously.

- Under the conditions for which bubble lattices were observed, the average size of the bubbles was equal in the αZr and βZr phases at the same fluence.

Application of TEM with *in situ* ion irradiation to different crystalline phases of zircaloy-4 has provided a useful means to investigate the effects of 6 keV He ions as a function of fluence and temperature. Further studies remain to be performed in order to understand the physical mechanisms that contribute to the formation of bubble lattices under irradiation at low and high temperatures and to confirm the proposed mechanisms for irradiation-assisted dissolution of Zr hydrides.

Acknowledgements

The authors are grateful to the Engineering and Physical Sciences Research Council (EPRSC) for funding the MIAMI-1 facility (grant number EP/E017266/1). MAT would like to thanks Dr. Houari Amari for useful discussions on HRTEM.

References

[1] H. Rickover, L. Geiger, B. Lustman, History of the development of zirconium alloys for use in nuclear reactors, Tech. rep., Energy Research and Development Administration, Washington, DC (USA). Div. of Naval Reactors (1975).

[2] A. Zaimovskii, Zirconium alloys in nuclear power, Atomic Energy 45 (6) (1978) 1165–1168.

[3] R. Pawel, J. Cathcart, R. McKee, The kinetics of oxidation of zircaloy-4 in steam at high temperatures, Journal of The Electrochemical Society 126 (7) (1979) 1105–1111.

[4] M. Griffiths, A review of microstructure evolution in zirconium alloys during irradiation, Journal of Nuclear Materials 159 (1988) 190–218. doi:10.1016/0022-3115(88)90093-1.
URL http://linkinghub.elsevier.com/retrieve/pii/0022311588900931

[5] R. B. Adamson, Effects of neutron irradiation on microstructure and properties of zircaloy, in: Zirconium in the Nuclear Industry: Twelfth International Symposium, ASTM International, 2000.

[6] C. Lemaignan, A. T. Motta, Zirconium alloys in nuclear applications, Materials science and technology.

[7] R. Gilbert, K. Farrell, C. Coleman, Damage structure in zirconium alloys neutron irradiated at 573 to 923 k, Journal of Nuclear Materials 84 (1-2) (1979) 137–148. doi:10.1016/0022-3115(79)90157-0.
URL http://linkinghub.elsevier.com/retrieve/pii/0022311579901570

[8] A. Jostsons, R. Blake, J. Napier, P. Kelly, K. Farrell, Faulted loops in neutron-irradiated zirconium, Journal of Nuclear Materials 68 (3) (1977) 267–276.

[9] M. Griffiths, R. Gilbert, V. Fidleris, R. Tucker, R. Adamson, Neutron damage in zirconium alloys irradiated at 644 to 710 k, Journal of Nuclear Materials 150 (2) (1987) 159–168. doi:10.1016/0022-3115(87)90071-7.
URL http://www.sciencedirect.com/science/article/pii/0022311587900717

[10] M. Griffiths, D. Gilbon, C. Regnard, C. Lemaignan, HVEM study of the effects of alloying elements and impurities on radiation damage in Zr-alloys, Journal of Nuclear Materials 205 (1993) 273–283. doi:10.1016/0022-3115(93)90090-L.
URL http://linkinghub.elsevier.com/retrieve/pii/002231159390090L

[11] D. Faulkner, C. Woo, Void swelling in zirconium, Journal of Nuclear Materials 90 (1-3) (1980) 307–316. doi:10.1016/0022-3115(80)90269-X.
URL http://linkinghub.elsevier.com/retrieve/pii/002231158090269X

[12] G. Was, Z. Jiao, E. Getto, K. Sun, A. Monterrosa, S. Maloy, O. Anderoglu, B. Sencer, M. Hackett, Emulation of reactor irradiation damage using ion beams, Scripta Materialia 88 (2014) 33–36. doi:10.1016/j.scriptamat.2014.06.003.
URL http://linkinghub.elsevier.com/retrieve/pii/S1359646214002243

[13] K. L. Murty, Materials Ageing and Degradation in Light Water Reactors: Mechanisms and Management, Elsevier, 2013.

[14] G. Was, J. Busby, T. Allen, E. Kenik, A. Jensson, S. Bruemmer, J. Gan, A. Edwards, P. Scott, P. Andreson, Emulation of neutron irradiation effects with protons: validation of principle, Journal of Nuclear Materials 300 (2-3) (2002) 198–216. doi:10.1016/S0022-3115(01)00751-6.
URL http://www.sciencedirect.com/science/article/pii/S0022311501007516

[15] S. E. Donnelly, The density and pressure of helium in bubbles in implanted metals: A critical review, Radiation Effects 90 (1-2) (1985) 1–47. doi:10.1080/00337578508222514.
URL http://www.tandfonline.com/doi/abs/10.1080/00337578508222514

[16] P. Edmondson, C. Parish, Y. Zhang, A. Hallén, M. Miller, Helium bubble distributions in a nanostructured ferritic alloy, Journal of Nuclear Materials 434 (1–3) (2013) 210 – 216, special Section on Spent Nuclear Fuel. doi:http://dx.doi.org/10.1016/j.jnucmat.2012.11.049.
URL http://www.sciencedirect.com/science/article/pii/S0022311512006447

[17] S. Sharafat, A. Takahashi, Q. Hu, N. Ghoniem, A description of bubble growth and gas release of helium implanted tungsten, Journal of Nuclear Materials 386-388 (2009) 900–903. doi:10.1016/j.jnucmat.2008.12.318.
URL http://www.sciencedirect.com/science/article/pii/S0022311508010155

[18] R. Harrison, H. Amari, G. Greaves, J. Hinks, S. Donnelly, Effect of he-appm/dpa ratio on the damage microstructure of tungsten, MRS Advances (2016) 1–7.

[19] R. Harrison, H. Amari, G. Greaves, S. Donnelly, J. Hinks, Tem with in situ ion irradiation of nuclear materials under in-service conditions, Microscopy and Microanalysis 22 (S3) (2016) 1460–1461.

[20] G. Rickers, G. Sørensen, Diffusion of inert gases in copper, physica status solidi (b) 32 (2) (1969) 597–608. doi:10.1002/pssb.19690320211.
URL http://dx.doi.org/10.1002/pssb.19690320211

[21] D. Ingram, D. Armour, High dose implantation of xenon into nickel, Nuclear Instruments and Methods in Physics Research 194 (1) (1982) 117 – 119. doi:http://dx.doi.org/10.1016/0029-554X(82)90500-6.
URL http://www.sciencedirect.com/science/article/pii/0029554X82905006

[22] J. Evans, D. Mazey, Evidence for solid krypton bubbles in copper, nickel and gold at 293k, Journal of Physics F: Metal Physics 15 (1) (1985) L1.

[23] D. Mazey, B. Eyre, J. Evans, S. Erents, G. McCracken, A transmission electron microscopy study of molybdenum irradiated with helium ions, Journal of Nuclear Materials 64 (1) (1977) 145 – 156. doi:http:

//dx.doi.org/10.1016/0022-3115(77)90018-6.
URL http://www.sciencedirect.com/science/article/pii/0022311577900186

[24] J. A. Hinks, S. J. Haigh, G. Greaves, F. Sweeney, C. T. Pan, R. J. Young, S. E. Donnelly, Dynamic microstructural evolution of graphite under displacing irradiation, Carbon 68 (2014) 273–284. doi:10.1016/j.carbon.2013.11.002.

[25] C. Yan, R. Wang, Y. Wang, X. Wang, G. Bai, Effects of ion irradiation on microstructure and properties of zirconium alloys-A review, Nuclear Engineering and Technology 47 (3) (2015) 323–331. doi:10.1016/j.net.2014.12.015.

[26] F. Onimus, J. Béchade, Radiation effects in zirconium alloys, Comprehensive Nuclear Materials 4 (2012) 31.

[27] G. Ran, J. Xu, Q. Shen, J. Zhang, N. Li, L. Wang, In situ TEM observation of growth behavior of Kr bubbles in zirconium alloy during post-implantation annealing, Nuclear Instruments and Methods in Physics Research Section B: Beam Interactions with Materials and Atoms 307 (2013) 516–521. doi:10.1016/j.nimb.2012.11.085.
URL http://www.sciencedirect.com/science/article/pii/S0168583X13001316

[28] L. Pagano, A. Motta, R. Birtcher, The formation of bubbles in Zr alloys under Kr ion irradiation, Journal of Nuclear Materials 244 (3) (1997) 295–304. doi:10.1016/S0022-3115(96)00757-X.
URL http://www.sciencedirect.com/science/article/pii/S002231159600757X

[29] R. Zee, J. Watters, O. Westcott, On the critical dose for blistering in helium irradiated zirconium and Zr-Nb, Journal of Nuclear Materials 115 (1) (1983) 131–133. doi:10.1016/0022-3115(83)90352-5.
URL http://www.sciencedirect.com/science/article/pii/0022311583903525http://linkinghub.elsevier.com/retrieve/pii/0022311583903525

[30] H. Shen, S. Peng, B. Chen, F. Naab, G. Sun, W. Zhou, X. Xiang, K. Sun, X. Zu, Helium bubble evolution in a Zr–Sn–Nb–Fe–Cr alloy during post-annealing: An in-situ investigation, Materials Characterization 107 (2015) 309–316. doi:10.1016/j.matchar.2015.07.025.
URL http://www.sciencedirect.com/science/article/pii/S104458031500282X

[31] B. Skinner, R. Dutton, Hydrogen diffusivity in α-β zirconium alloys and its role in delayed hydride cracking, 1990.

[32] S. Sagat, C. Coleman, M. Griffiths, B. Wilkins, Zirconium in the Nuclear Industry: Tenth International Symposium, ASTM International, 100 Barr Harbor Drive, PO Box C700, West Conshohocken, PA 19428-2959, 1994. doi:10.1520/STP1245-EB.
URL http://www.astm.org/DIGITAL{_}LIBRARY/STP/PAGES/STP15183S.htm

[33] D. O. Northwood, U. Kosasih, Hydrides and delayed hydrogen cracking in zirconium and its alloys, International Metals Reviews 28 (1) (2013) 92–121. doi:10.1179/imtr.1983.28.1.92.
URL http://www.tandfonline.com/doi/abs/10.1179/imtr.1983.28.1.92

[34] J. Bair, M. A. Zaeem, M. Tonks, A Review on Hydride Precipitation in Zirconium Alloys, Journal of Nuclear Materials 466 (2015) 12–20. doi:10.1016/j.jnucmat.2015.07.014.
URL http://www.sciencedirect.com/science/article/pii/S0022311515301008

[35] J. Bai, C. Prioul, D. Francois, Hydride embrittlement in zircaloy-4 plate: Part i. influence of microstructure on the hydride embrittlement in zircaloy-4 at 20 c and 350 c, Metallurgical and materials transactions A 25 (6) (1994) 1185–1197.

[36] B. de Gabory, A. T. Motta, K. Wang, Transmission electron microscopy characterization of Zircaloy-4 and ZIRLO^{TM} oxide layers, Journal of Nuclear Materials 456 (2015) 272–280. doi:10.1016/j.jnucmat.2014.09.073.
URL http://linkinghub.elsevier.com/retrieve/pii/S0022311514006734

[37] W. M. Mueller, J. P. Blackledge, G. G. Libowitz, Metal hydrides, Elsevier, 2013.

[38] J. Bradbrook, G. Lorimer, N. Ridley, The precipitation of zirconium hydride in zirconium and zircaloy-2, Journal of Nuclear Materials 42 (2) (1972) 142–160.

[39] G. Carpenter, J. Watters, An in-situ study of the dissolution of γ-zirconium hydride in zirconium, Journal of Nuclear Materials 73 (2) (1978) 190–197. doi:10.1016/0022-3115(78)90559-7.
URL http://www.sciencedirect.com/science/article/pii/0022311578905597

[40] D. Northwood, R. Gilbert, L. Bahen, P. Kelly, R. Blake, A. Jostsons, P. Madden, D. Faulkner, W. Bell, R. Adamson, Characterization of neutron irradiation damage in zirconium alloys — an international "round-robin" experiment, Journal of Nuclear Materials 79 (2) (1979) 379–394. doi:10.1016/0022-3115(79)90103-X.
URL http://www.sciencedirect.com/science/article/pii/002231157990103X

[41] J. Hinks, J. Van Den Berg, S. Donnelly, Miami: Microscope and ion accelerator for materials investigations, Journal of Vacuum Science & Technology A: Vacuum, Surfaces, and Films 29 (2) (2011) 021003.

[42] C. A. Schneider, W. S. Rasband, K. W. Eliceiri, Nih image to imagej: 25 years of image analysis, Nature methods 9 (7) (2012) 671.

[43] J. F. Ziegler, M. D. Ziegler, J. P. Biersack, Srim–the stopping and range of ions in matter (2010), Nuclear Instruments and Methods in Physics Research Section B: Beam Interactions with Materials and Atoms 268 (11) (2010) 1818–1823.

[44] R. Stoller, M. Toloczko, G. Was, A. Certain, S. Dwaraknath, F. Garner, On the use of SRIM for computing radiation damage exposure, Nuclear Instruments and Methods in Physics Research Section B: Beam Interactions with Materials and Atoms 310 (2013) 75–80. doi:10.1016/j.nimb.2013.05.008.
URL http://www.sciencedirect.com/science/article/pii/S0168583X13005053

[45] ICDD, Pcpdfwin software - jcpds powder diffraction, Joint Committee on Powder Diffraction Standards–International Centre for Diffraction Data, Swarthmore, USA.

[46] B. Fultz, J. M. Howe, Transmission electron microscopy and diffractometry of materials, Springer Science & Business Media, 2012.

[47] G. Carpenter, J. Watters, Electron diffraction patterns for hcp Zr, Tech. rep., Chalk River Nuclear Laboratories (1972).

[48] E. Zuzek, J. Abriata, A. San-Martin, F. Manchester, The h-zr (hydrogen-zirconium) system, Bulletin of alloy phase diagrams 11 (4) (1990) 385–395.

[49] N. Nieva, D. Arias, Experimental partial phase diagram of the zr–sn–fe system, Journal of nuclear materials 359 (1) (2006) 29–40.

[50] H. K. Birnbaum, Mechanisms of hydrogen related fracture of metals, Tech. rep., DTIC Document (1989).

[51] B. Cox, Some thoughts on the mechanisms of in-reactor corrosion of zirconium alloys, Journal of Nuclear Materials 336 (2-3) (2005) 331–368. doi:10.1016/j.jnucmat.2004.09.029.
URL http://www.sciencedirect.com/science/article/pii/S002231150400875X

[52] H. Trinkaus, B. Singh, Helium accumulation in metals during irradiation – where do we stand?, Journal of Nuclear Materials 323 (2-3) (2003) 229–242. doi:10.1016/j.jnucmat.2003.09.001.
URL http://www.sciencedirect.com/science/article/pii/S0022311503004033

[53] S. Sass, B. Eyre, Diffraction from void and bubble arrays in irradiated molybdenum, Philosophical Magazine 27 (6) (1973) 1447–1453.

[54] J. Evans, Void and bubble lattice formation in molybdenum: A mechanism based on two-dimensional self-interstitial diffusion, Journal of Nuclear Materials 119 (2-3) (1983) 180–188. doi:10.1016/0022-3115(83)90195-2.

[55] J. Evans, Irradiation-induced cavity lattice formation in metals, in: Patterns, Defects and Materials Instabilities, Springer, 1990, pp. 347–370.

[56] J. Evans, A. Foreman, R. McElroy, Anisotropic diffusion of self-interstitials in zirconium, Journal of Nuclear Materials 168 (3) (1989) 340–342.

[57] J. Evans, Comments on the role of 1-D and 2-D self-interstitial atom transport mechanisms in void- and bubble-lattice formation in cubic metals, Philosophical Magazine Letters 87 (8) (2007) 575–580. doi:

10.1080/09500830701393148.

[58] J. H. Evans, Simulations of the effects of 2-D interstitial diffusion on void lattice formation during irradiation, Philosophical Magazine 86 (2) (2006) 173–188. doi:10.1080/14786430500380134.
URL http://www.tandfonline.com/doi/abs/10.1080/14786430500380134

[59] M. W. Thompson, Defects and radiation damage in metals, Defects and Radiation Damage in Metals, by MW Thompson, Cambridge, UK: Cambridge University Press, 1974 1.

[60] A. J. E. Foreman, B. N. Singh, Bubble nucleation in grain interior and its influence on helium accumulation at grain boundaries, Journal of Nuclear Materials 133-134 (C) (1985) 451–454. doi:10.1016/0022-3115(85)90187-4.
URL http://www.sciencedirect.com/science/article/pii/0022311585901874

[61] F. Willaime, A. Satta, M. Nastar, O. Le Bacq, Electronic structure calculations of vacancy parameters in transition metals: Impact on the bcc self-diffusion anomaly, International Journal of Quantum Chemistry 77 (6) (2000) 927–939. doi:10.1002/(SICI)1097-461X(2000)77:6<927::AID-QUA1>3.0.CO;2-5.

Contents

List of Figures

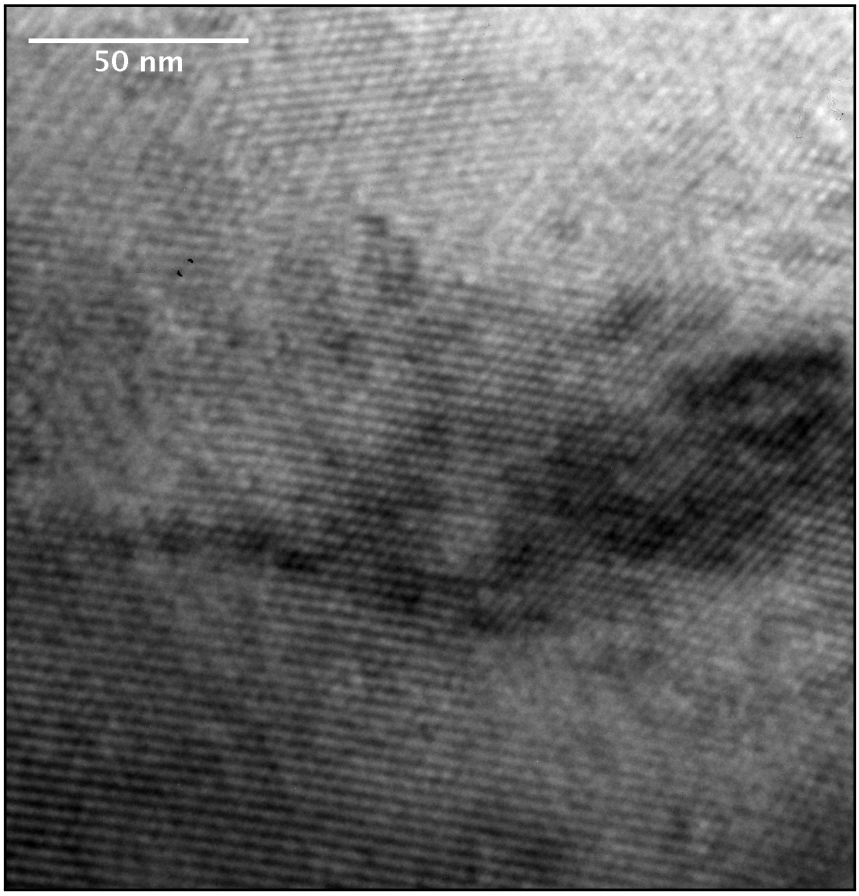

Figure 1: High-resolution TEM image obtained at room temperature from an electropolished sample of zircaloy-4.

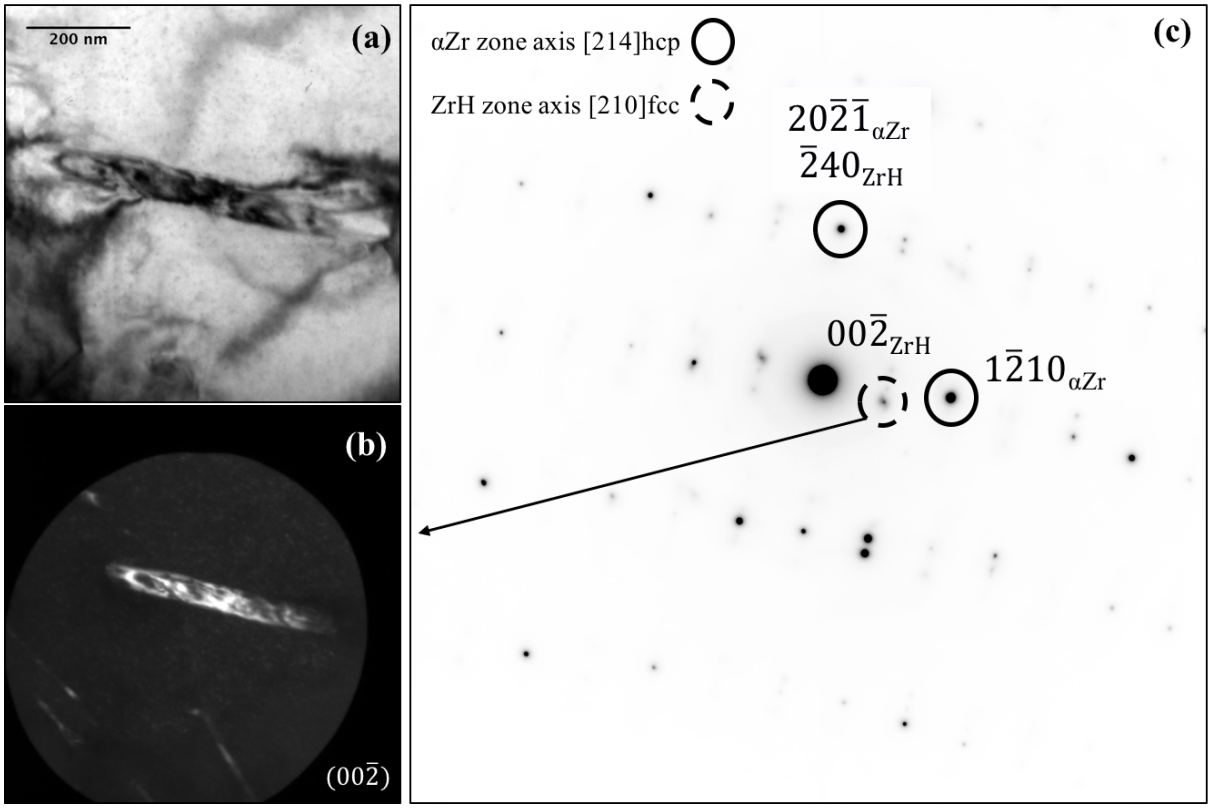

Figure 2: Hydride characterisation with (a) bright-field image, (b) dark-field image formed using the (00$\bar{2}$) hydride reflection and (c) a FCC diffraction pattern (from the hydride) mixed with the HCP crystal structure corresponding to the parent phase. The scale marker in (a) applies to both micrographs.

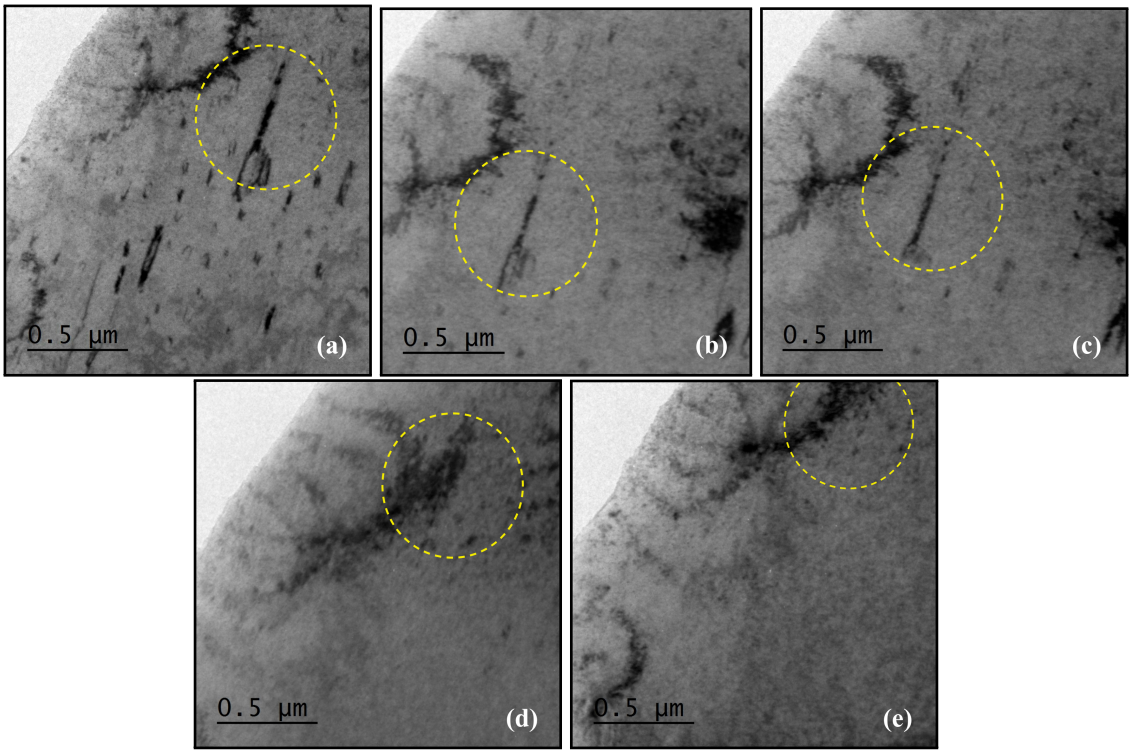

Figure 3: *In-situ* annealing of zircaloy-4 showing hydride dissolution between room temperature and 1148 K: (a) room temperature; (b) t = 4 s during the temperature ramp; (c) t = 8 s; (d) t = 10 s at ≈ 823 K; (e) microstructure at 1148 K. The images have been extracted from a video recorded during *in situ* TEM heating and therefore the field of view varies slightly due to thermal drift.

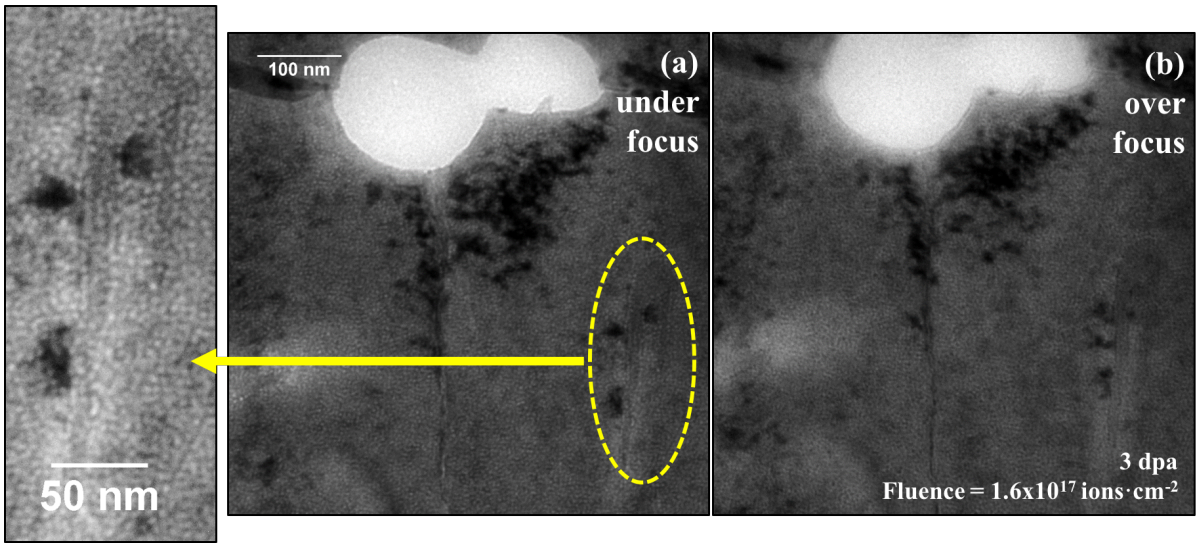

Figure 4: TEM images captured in (a) bright-field under-focused conditions and (b) bright-field over-focused conditions of the microstructure of zircaloy-4 irradiated at room temperature (298 K). The dashed ellipse highlights the accumulation of He bubbles on the boundary of a hydride. The scale marker in (a) also applies to (b).

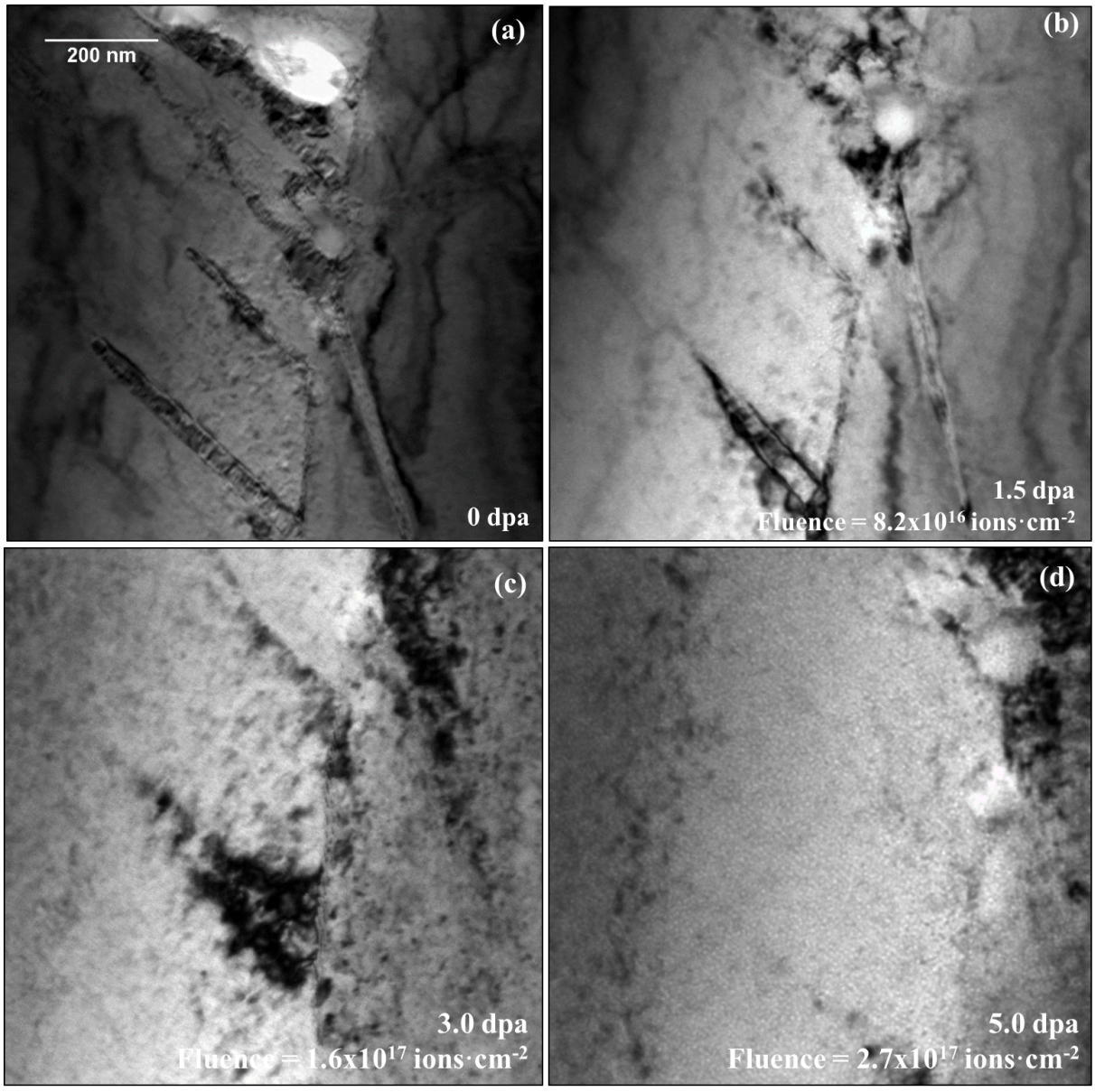

Figure 5: TEM images of hydrides dissolving under 6 keV He irradiation at 473 K: (a) prior to irradiation; (b-c) hydrides dissolving; and (d) the resulting microstructure after irradiation exhibiting a high areal density of He bubbles. The scale marker in (a) applies to all the micrographs in the figure.

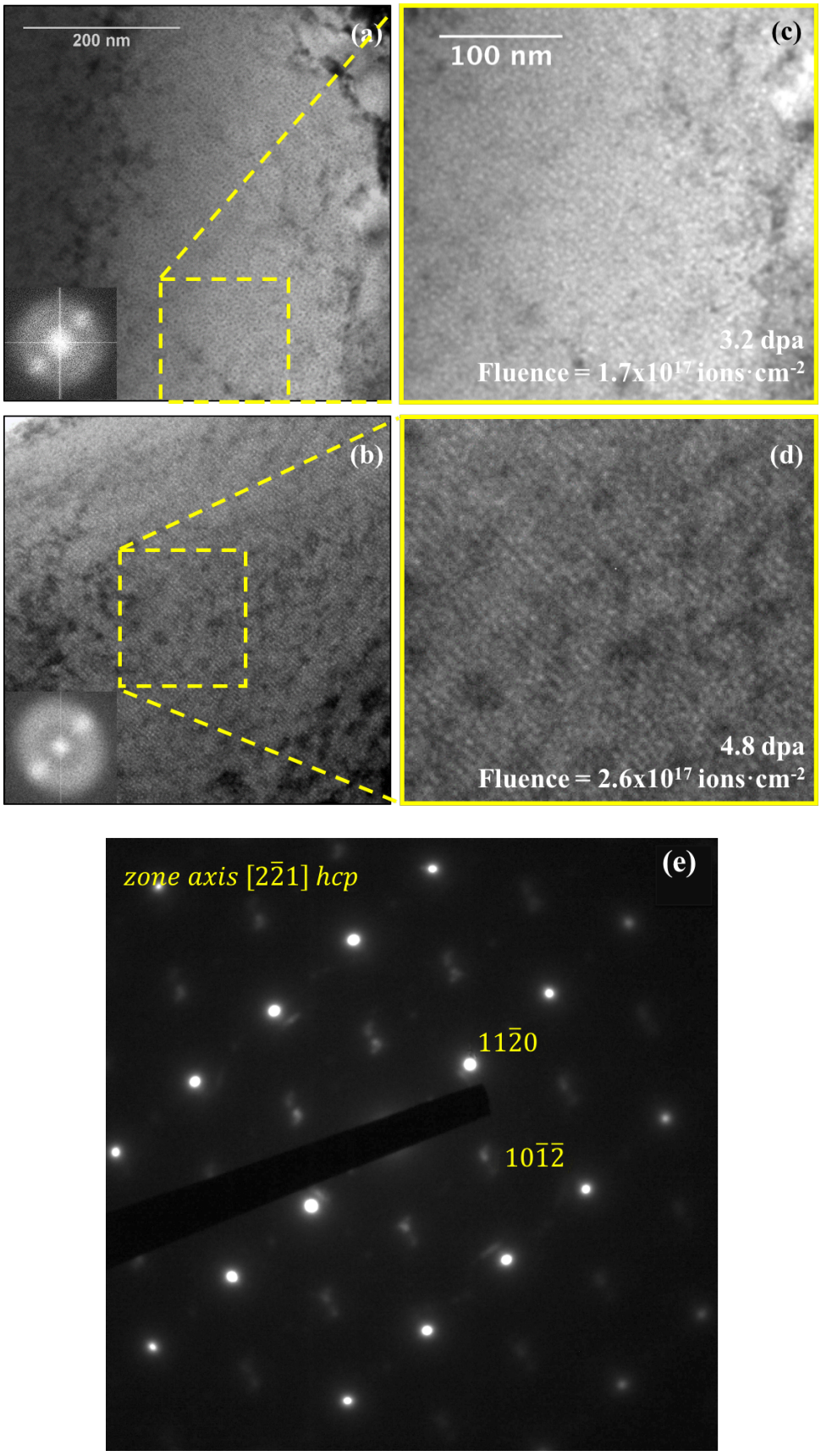

Figure 6: Bubble lattices at 473 K: (a) at 3.2 dpa and (b) at 4.8 dpa. The diffraction pattern (e) confirms the αZr phase. The FFT insets in (a) and (b) exhibit bright lobes confirming the bubble lattice periodicity. The scale marker in (a) also applies to (b) and the marker in (c) also applies to (d).

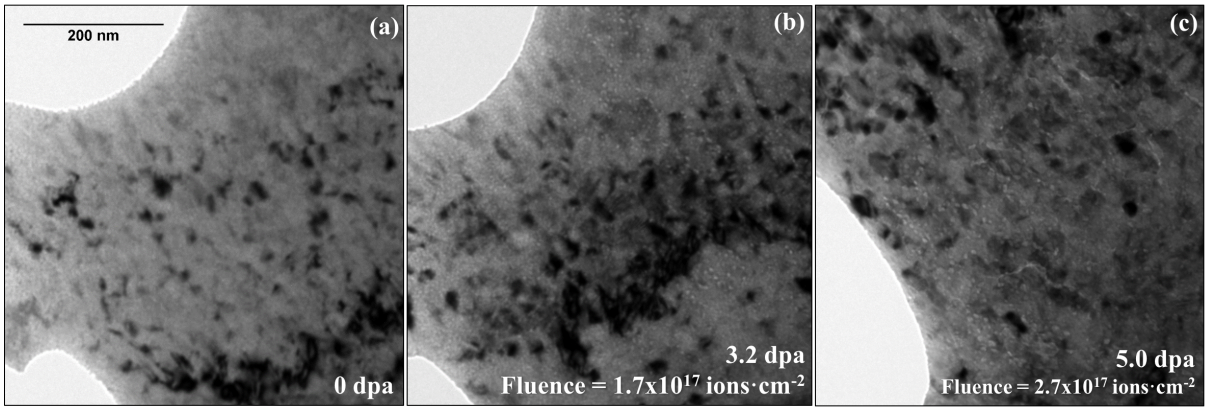

Figure 7: Bubble evolution as a function of fluence in zircaloy-4 implanted with 6 keV He at 973 K: (a) 0 dpa, (b) 1.7×10^{17}ions $\cdot$ cm^{-2} (3.2 dpa) and (c) 2.7×10^{17}ions $\cdot$ cm^{-2} (5.0 dpa). The scale marker in (a) applies to all the micrographs in the figure.

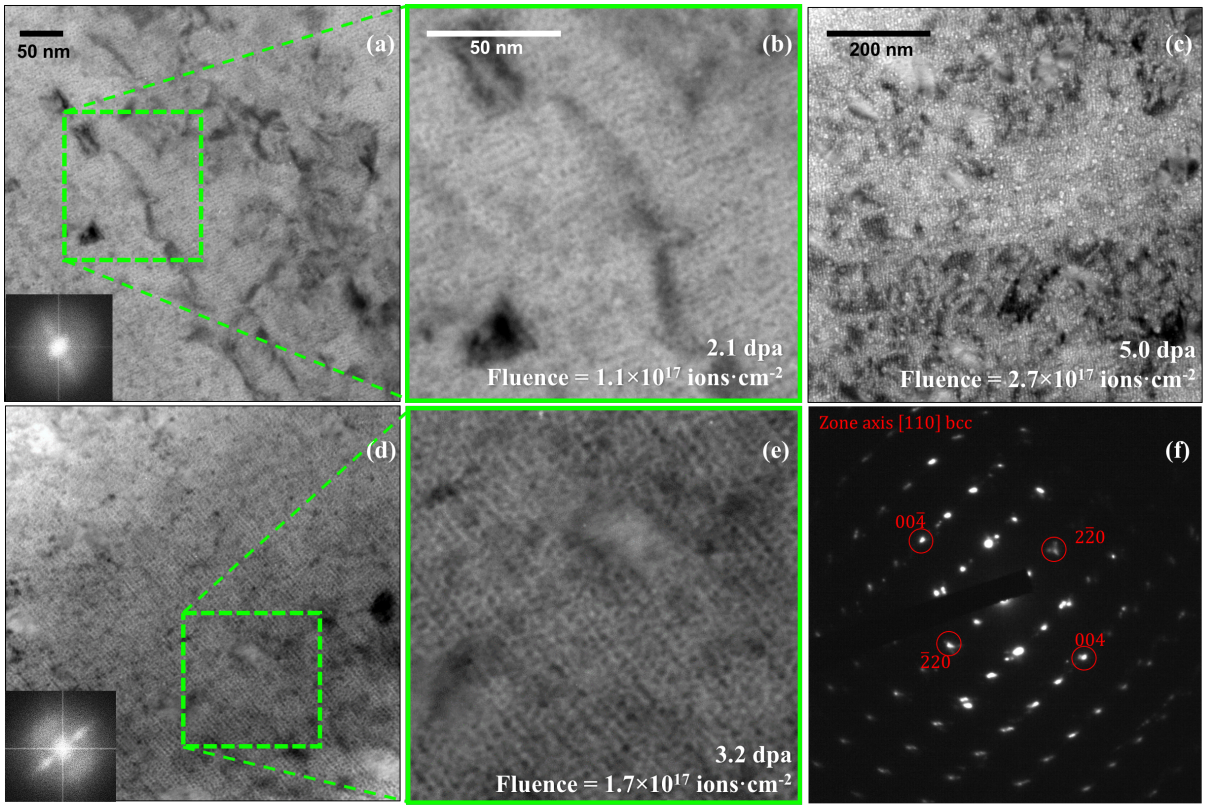

Figure 8: TEM micrographs of zircaloy-4 microstructure irradiated using 6 keV He ions at 1148 K showing (a) an example of a bubble lattice at 1.1×10^{17}ions $\cdot$ cm^{-2} (2.1 dpa) and at a (d) 1.7×10^{17}ions $\cdot$ cm^{-2} (3.2 dpa) with (f) the diffraction pattern confirming the βZr phase. Coalescence of bubbles (c) was observed at 2.7×10^{17}ions $\cdot$ cm^{-2} (5.0 dpa). The scale marker in (a) also applies to (d) and the marker in (b) also applies to (e).

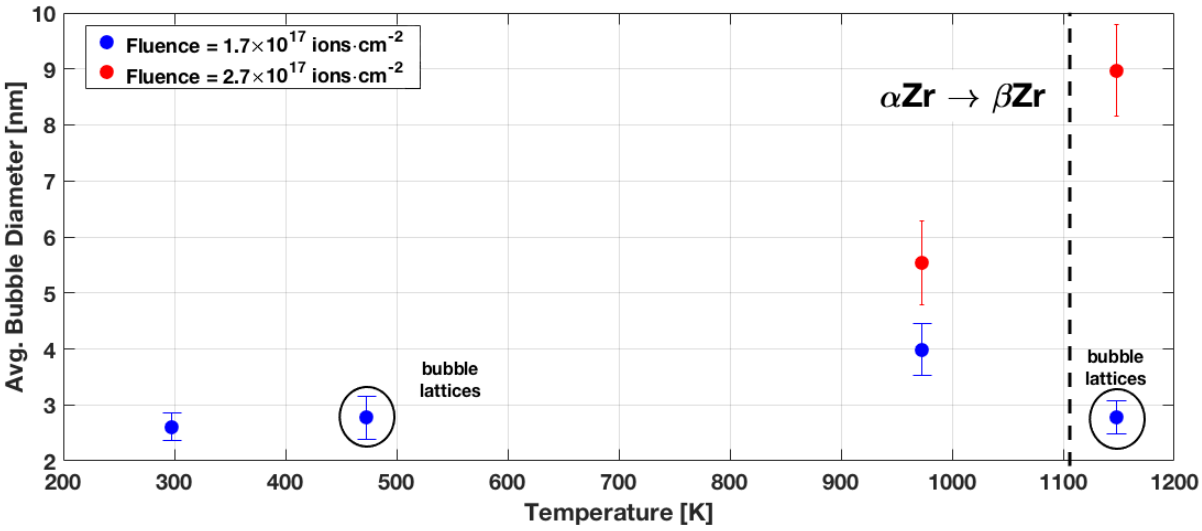

Figure 9: Bubble size versus implantation temperature of zircaloy-4 irradiated with 6 keV He ions. The error bars in the vertical axis are the standard deviations from the statistical analysis.

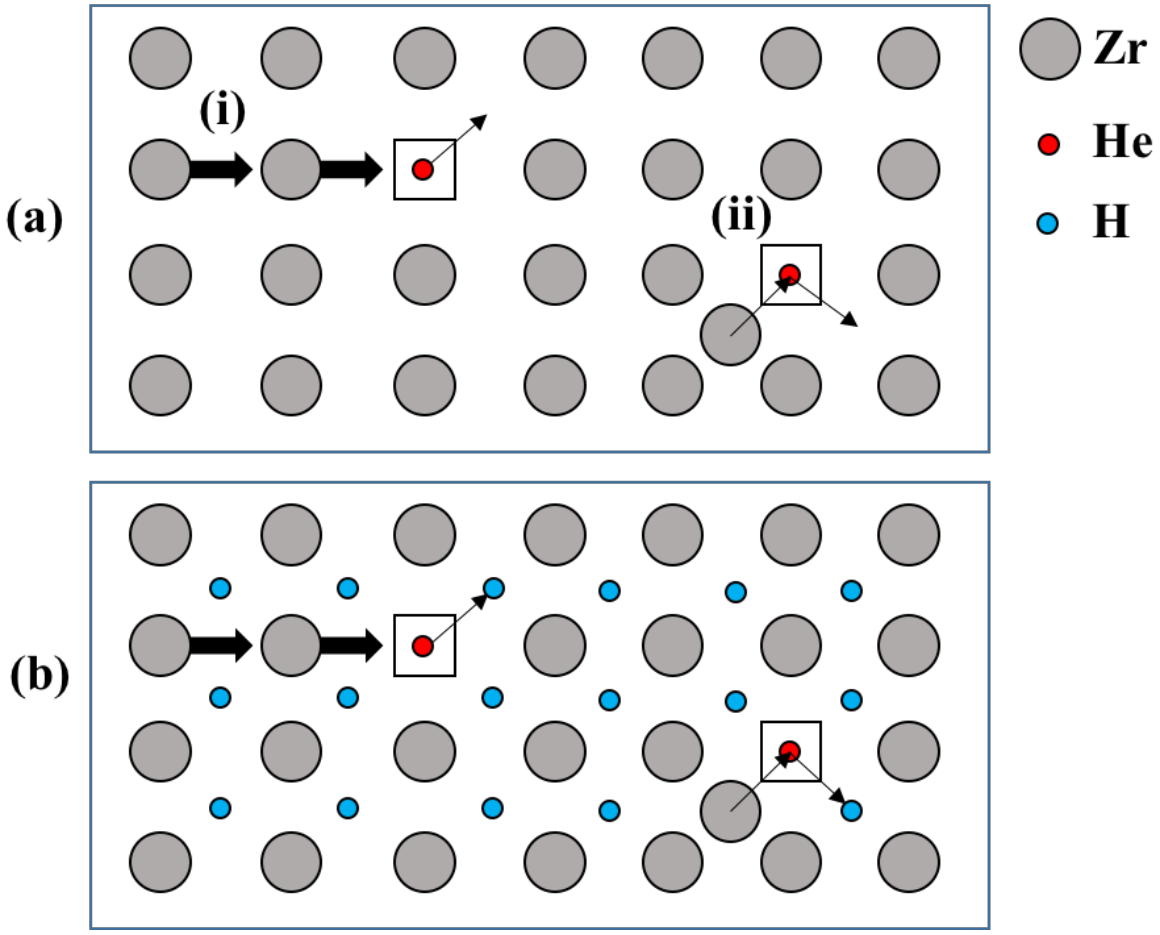

Figure 10: (a) Diffusion mechanisms of He in the Zr matrix [52]: (i) a collisional displacement and (ii) a replacement event. (b) The equivalent mechanisms in the ZrH microstructure which can remove H atoms from solid solution leading to hydride irradiation-assisted dissolution.